The fine structure of two-electron states in single and double quantum dots



2010 J. Phys.: Condens. Matter 22 025301

(http://iopscience.iop.org/0953-8984/22/2/025301)

J. Phys.: Condens. Matter **22** (2010) 025301 (9pp) doi:10.1088/0953-8984/22/2/025301

# The fine structure of two-electron states in single and double quantum dots

**M M Glazov**

Ioffe Physical-Technical Institute RAS, 194021 St Petersburg, Russia

Received 3 September 2009, in final form 22 October 2009
Published 9 December 2009
Online at stacks.iop.org/JPhysCM/22/025301

**Abstract**

The energy spectrum fine structure of triplet two-electron states in nanostructures is investigated theoretically. Spin–orbit interaction-induced terms in the effective Hamiltonian of the electron–electron interaction are derived for zinc blende lattice semiconductor systems: quantum wells and quantum dots. The effects of bulk and structural inversion asymmetry are taken into account. Simple analytical expressions describing the splittings of the two-electron states localized in a single quantum dot and in a lateral double quantum dot are derived. The spin degeneracy of triplet states is shown to be completely lifted by the spin–orbit interaction. An interplay of the conduction band spin splitting and the spin–orbit terms in the electron–electron interaction is discussed. The emission spectra of hot trions and of doubly charged excitons are calculated and are shown to reveal the fine structure of two-electron states.

(Some figures in this article are in colour only in the electronic version)

## 1. Introduction

Semiconductor quantum dots (QDs), also known as artificial atoms, demonstrate unique spin-dependent properties and have a strong potential for spintronics [1]. The fine structure of optical emission spectra of QDs provides detailed information on the charge carriers' energy spectrum and their interactions [2].

The fine structure of neutral QD energy spectra and, hence, their luminescence spectra are determined by the exchange interaction between an electron and a hole forming a zero-dimensional exciton [2]. The situation is different in the case of doped QDs: for instance, in $n$-type singly charged QDs the emission is dominated by $X^-$ trions consisting of two electrons and a hole, and in doubly charged QDs the emission involves the transition from the state with three electrons and one hole ($X^{2-}$) into the state with two electrons [3–6]. On these occasions, the fine structure of optical spectra is controlled also by the exchange interaction between electrons.

It is well known that two-electron states are split into spin singlet and triplet states by the exchange Coulomb interaction. In the absence of the spin–orbit interaction, the triplet states are degenerate. It was demonstrated recently that the spin–orbit contribution to the electron–electron interaction (*spin–orbit exchange interaction*) splits a two-electron triplet state into three sublevels, one of which corresponds to zero projection of the total spin on the growth axis and two others correspond to the linear combinations of the states with the total spin projections being $\pm 1$, similar to those of localized excitons [7].

Here we extend the theory developed in [7] to allow for the full microscopic symmetry of real QDs made of zinc blende lattice semiconductors. The effects of the bulk inversion asymmetry caused by the absence of an inversion center in the point symmetry group of a zinc blende lattice and of the structural inversion asymmetry on the fine structure of two-electron triplet states are analyzed. The developed theory is applied to calculate the two-electron states and emission spectra of a hot trion and $X^{2-}$ complex in single and double QDs.

## 2. Model

In what follows we consider quantum discs (quantum well QDs) and lateral double QDs grown from zinc blende lattice direct-gap materials. It is convenient to (i) obtain the spin–orbit contributions to an effective Hamiltonian of the electron–electron interaction in a quantum well and (ii) calculate the fine structure of the two-electron states localized in the quantum well plane using the derived Hamiltonian.

The schematic band structure of the direct band zinc blende lattice semiconductor is depicted in figure 1(a). The spin–orbit interaction for the conduction band ($\Gamma_6^c$) electrons is largely determined by the $\boldsymbol{k}\cdot\boldsymbol{p}$ admixture of the valence band states ($\Gamma_8^v$, $\Gamma_7^v$). The effects due to the lack of an

 

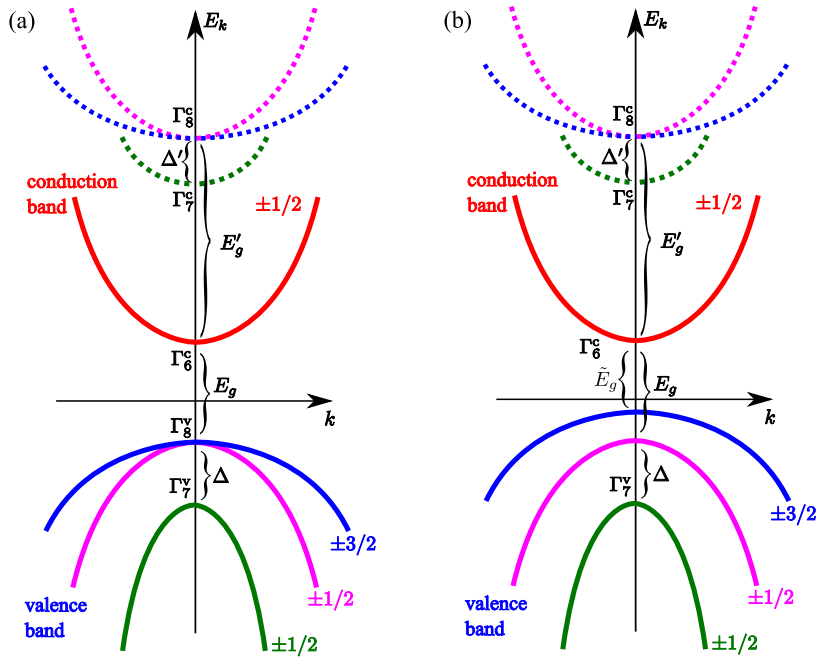


**Figure 1.** (a) Schematic illustration of the band structure of a direct band zinc blende lattice-based semiconductor. (b) Schematic illustration of the band structure of a uniaxially deformed zinc blende lattice-based semiconductor. Splittings are not shown to scale.

inversion center in the point symmetry group of the bulk material disregarded in [7] can be taken into account by taking into consideration the remote conduction bands $\Gamma_8^c$ and $\Gamma_7^c$.

Under the assumption that the gap $E_g'$ between the $\Gamma_6^c$ and $\Gamma_8^c$ exceeds by far the bandgap $E_g$ (between $\Gamma_6^c$ and $\Gamma_8^v$) and that the spin–orbit splitting $\Delta'$ of the $\Gamma_8^c$, $\Gamma_7^c$ bands is much smaller as compared with $E_g'$, the band structure can be treated within the framework of the extended eight-band Kane model by including terms quadratic in the wavevector into the off-diagonal matrix elements characterizing the $\boldsymbol{k}\cdot\boldsymbol{p}$ interaction of the valence band states with the conduction band states [8].

The free-electron wavefunction in a quantum well grown along the $z \parallel [001]$ axis can be represented as (cf [7])

$$\Psi_{s,k}(\boldsymbol{\rho}, z) = \mathrm{e}^{\mathrm{i}k\rho}[\mathsf{S}_r + \mathrm{i}\mathbf{R}_r\cdot(A\hat{\boldsymbol{\kappa}}_K - \mathrm{i}B\hat{\boldsymbol{\sigma}}\times\hat{\boldsymbol{\kappa}}_K)]\varphi(z)|\chi_s\rangle. \quad (1)$$

Here $\boldsymbol{r} = (\boldsymbol{\rho}, z)$ is the electron position vector, $\varphi(z)$ is the smooth envelope describing its size quantization along the $z$ axis, $\hat{\boldsymbol{\sigma}}$ is the electron spin operator, $\mathsf{S}_r$ and $\mathbf{R}_r = (\mathsf{X}_r^v, \mathsf{Y}_r^v, \mathsf{Z}_r^v)$ are $s$-type and $p$-type Bloch functions of the conduction and valence bands, respectively, taken at the $\Gamma$ point, $|\chi_s\rangle$ is a spinor, $A = P(3E_g + 2\Delta)/[3E_g(E_g + \Delta)]$ and $B = -P\Delta/[3E_g(E_g + \Delta)]$, $\Delta$ is the gap $\Gamma_8^v$–$\Gamma_7^v$ and $P$ is the Kane parameter. Equation (1) is valid provided that the electron energy referred to the conduction band bottom is much smaller compared to $E_g$ and $\Delta$.

The vector $\hat{\boldsymbol{\kappa}}_K$ describing the admixture of the valence bands has the following Cartesian components in the cubic axes $x \parallel [100]$ and $y \parallel [010]$:

$$\hat{\boldsymbol{\kappa}}_{K,i} = \hat{K}_i - \mathrm{i}\beta\hat{K}_{i+1}\hat{K}_{i+2}, \quad (2)$$

where $\hat{\boldsymbol{K}} = (\boldsymbol{k}, -\mathrm{i}\partial/\partial z)$ is the wavevector of the electron, a cyclic rule is applied for the subscripts $(i + 3 = i)$ and the constant $\beta$ can be related to the bulk Dresselhaus parameter $\gamma_c$ describing cubic in $k$ conduction band spin splitting as $\beta = \gamma_c/2BP$ [8, 9]. In [7] the quadratic in the wavevector contributions to equation (2) were disregarded. These terms, being even in the wavevector components, arise in the systems with bulk inversion asymmetry only, and they are caused by the mixing between $\Gamma_7^c$ and $\Gamma_8^c$ bands, and $\Gamma_7^v$ and $\Gamma_8^v$ bands, see figure 1.

The matrix elements of the effective electron–electron interaction Hamiltonian taken between the states $(\boldsymbol{k}s, \boldsymbol{k}'s')$ and $(\boldsymbol{p}s_1, \boldsymbol{p}'s_1')$, $M(\boldsymbol{k}s, \boldsymbol{k}'s' \to \boldsymbol{p}s_1, \boldsymbol{p}'s_1')$, are calculated following the procedure outlined in [7]. They can be efficiently expressed in terms of a function $\hat{\mu}(z, \boldsymbol{k} \to \boldsymbol{p}, \hat{\boldsymbol{\sigma}})$ which is

$$\begin{aligned}\hat{\mu}(z, \boldsymbol{k} \to \boldsymbol{p}, \hat{\boldsymbol{\sigma}}) = {} & \varphi^2(z) + \mathrm{i}\xi\{\hat{\sigma}_z[\boldsymbol{p}\times\boldsymbol{k}]\varphi^2(z) \\ & - \mathrm{i}[\hat{\boldsymbol{\sigma}}\times(\boldsymbol{p}+\boldsymbol{k})]_z\varphi'(z)\varphi(z) \\ & + \mathrm{i}\beta[\hat{\sigma}_x(p_x+k_x) - \hat{\sigma}_y(p_y+k_y)][\varphi'(z)]^2 \\ & - \mathrm{i}\beta[\hat{\sigma}_x p_y k_y(p_x+k_x) - \hat{\sigma}_y p_x k_x(p_y+k_y)]\varphi^2(z)\}, \end{aligned} \quad (3)$$

where the parameter $\xi$,

$$\xi = 2AB + B^2 = -\frac{P^2}{3}\frac{\Delta(2E_g+\Delta)}{E_g^2(E_g+\Delta)^2}, \quad (4)$$

characterizes the strength of the spin–orbit interaction. Its values for some semiconductors are given in table 1. Here we neglected the corrections to the first three terms in equation (3) caused by the electron energy spectrum non-parabolicity. The terms proportional to $\beta$ are caused by the bulk inversion asymmetry and arise from the quadratic in wavevector contributions to $\hat{\boldsymbol{\kappa}}_k$.

Finally

$$\begin{aligned} M(\boldsymbol{k}s, \boldsymbol{k}'s' \to \boldsymbol{p}s_1, \boldsymbol{p}'s_1') = {} & \delta_{k+k',p+p'} \\ & \times \int \mathrm{d}z_1\,\mathrm{d}z_2 V(\boldsymbol{p}-\boldsymbol{k}, z_1 - z_2)\langle\chi_{s_1}\chi_{s_1'}|\hat{\mu} \\ & \times (z_1, \boldsymbol{k} \to \boldsymbol{p}, \hat{\boldsymbol{\sigma}}^{(1)})\hat{\mu}(z_2, \boldsymbol{k}' \to \boldsymbol{p}', \hat{\boldsymbol{\sigma}}^{(2)})|\chi_s\chi_{s'}\rangle. \end{aligned} \quad (5)$$

**Table 1.** Spin–orbit interaction strength $\xi$ [10].

| Material | $\xi$ (Å$^2$) |
|---|---|
| GaAs | 5 |
| InAs | 100 |
| InSb | 500 |
| CdSe | 3 |
| CdTe | 5 |
| ZnTe | 2 |

Here $V(q,z) = \Xi^{-1}\int V(r)\mathrm{e}^{-\mathrm{i}q\rho}\mathrm{d}\rho$, where $V(r) = e^2/(\varkappa r)$ is the Coulomb potential, $\varkappa$ is the static dielectric constant, $\Xi$ is the normalization area, $q = p - k$ is the transferred wavevector, and $\hat{\sigma}^{(1)}$ and $\hat{\sigma}^{(2)}$ are the spin operators of the first and second electrons (acting on spinors $|\chi_s\rangle$, $|\chi_{s_1}\rangle$ and on $|\chi_{s'}\rangle$, $|\chi_{s'_1}\rangle$, respectively). Note that the matrix element equation (5) is derived for not (anti)symmetrized wavefunctions, cf [11].

One can represent the matrix element equation (5) as a sum of spin–orbit independent contributions, $M^{(0)}$, the contributions linear in spin operators $\hat{\sigma}^{(1)}$ and $\hat{\sigma}^{(2)}$, $M^{(1)}$, and the quadratic in spin operator terms, $M^{(2)}$.

In what follows we consider a simple model of the quantum well of width $d$ with infinite barriers. The electron envelope function for the lowest size-quantization subband is taken in the form

$$\varphi(z) = \sqrt{\frac{2}{d}}\left[\cos\left(\frac{\pi z}{d}\right) + \alpha\sin\left(\frac{2\pi z}{d}\right)\right], \quad -d/2 \leqslant z \leqslant d/2. \tag{6}$$

The possible quantum well heteropotential asymmetry (i.e. structural inversion asymmetry) is taken into account by the second term in the square brackets; it is assumed that $\alpha \ll 1$.

The spin–orbit independent contribution is given by the Fourier transform of the quasi-two-dimensional Coulomb potential [12]:

$$M^{(0)}(\boldsymbol{k}s, \boldsymbol{k}'s' \to \boldsymbol{p}s_1, \boldsymbol{p}'s'_1) = \frac{2\pi e^2}{\Xi\varkappa q}\delta_{\boldsymbol{k}+\boldsymbol{k}',\boldsymbol{p}+\boldsymbol{p}'}\delta_{s,s_1}\delta_{s',s'_1}F_{22}^{00}(q), \tag{7}$$

with $F_{22}^{00}(q) = 1$ at $qd \ll 1$ (the definition of the form factors $F_{ij}^{kl}$ is given in [7]).

The linear in spin operators' contributions are responsible for the asymmetric scattering. They are proportional to $\xi$ and are

$$\begin{aligned} M^{(1)}(\boldsymbol{k}s, \boldsymbol{k}'s' \to \boldsymbol{p}s_1, \boldsymbol{p}'s'_1) = {} & \xi\frac{2\pi e^2}{\Xi\varkappa q}\delta_{\boldsymbol{k}+\boldsymbol{k}',\boldsymbol{p}+\boldsymbol{p}'} \\ & \times \langle\chi_{s_1}\chi_{s'_1}|[\hat{\boldsymbol{\sigma}}^{(1)}\times(\boldsymbol{p}+\boldsymbol{k})]_z F_{12}^{10}(q) \\ & + [\hat{\boldsymbol{\sigma}}^{(2)}\times(\boldsymbol{p}'+\boldsymbol{k}')]_z F_{21}^{01}(q) \\ & - \beta[\hat{\sigma}_x^{(1)}(p_x+k_x) - \hat{\sigma}_y^{(1)}(p_y+k_y)]F_{02}^{20}(q) \\ & - \beta[\hat{\sigma}_x^{(2)}(p'_x+k'_x) - \hat{\sigma}_y^{(2)}(p'_y+k'_y)]F_{20}^{02}(q) \\ & + \mathrm{i}\hat{\sigma}_z^{(1)}[\boldsymbol{p}\times\boldsymbol{k}]_z F_{22}^{00}(q) + \mathrm{i}\hat{\sigma}_z^{(2)}[\boldsymbol{p}'\times\boldsymbol{k}']_z F_{22}^{00}(q)|\chi_s\chi_{s'}\rangle. \end{aligned} \tag{8}$$

Here we retained only linear and quadratic in wavevectors terms. The second and third lines in equation (8) describe Rashba-like contributions to electron–electron scattering similar to the structural inversion asymmetry terms in electron impurity or electron phonon scattering [13, 14]. However, the form factors $F_{12}^{10} = F_{21}^{01} \equiv 0$ in our model and structural inversion asymmetry terms vanish[1]. In equation (8) terms $\propto\beta$ describe bulk inversion asymmetry effects, these contributions having the form similar to the Dresselhaus Hamiltonian [13]. The corresponding form factors are $F_{02}^{20}(q) = F_{20}^{02}(q) = \pi^2/d^2$ at $qd \ll 1$. Finally, the last line describes Mott (skew) scattering. These linear in spin terms can cause the spin currents generation due to electron–electron interaction [15].

The quadratic in spin operator terms describe spin–spin interaction and can be written as

$$\begin{aligned} M^{(2)}(\boldsymbol{k}s, \boldsymbol{k}'s' \to \boldsymbol{p}s_1, \boldsymbol{p}'s'_1) = {} & \xi^2\frac{2\pi e^2}{\Xi\varkappa q}\delta_{\boldsymbol{k}+\boldsymbol{k}',\boldsymbol{p}+\boldsymbol{p}'} \\ & \times \langle\chi_{s_1}\chi_{s'_1}|\{[\hat{\boldsymbol{\sigma}}^{(1)}\times(\boldsymbol{p}+\boldsymbol{k})]_z[\hat{\boldsymbol{\sigma}}^{(2)}\times(\boldsymbol{p}'+\boldsymbol{k}')]_z F_{11}^{11}(q) \\ & + \beta^2[\hat{\sigma}_x^{(1)}(p_x+k_x) - \hat{\sigma}_y^{(1)}(p_y+k_y)] \\ & \times [\hat{\sigma}_x^{(2)}(p'_x+k'_x) - \hat{\sigma}_y^{(2)}(p'_y+k'_y)]F_{00}^{22}(q) \\ & - \beta[\hat{\sigma}_x^{(1)}(p_x+k_x) - \hat{\sigma}_y^{(1)}(p_y+k_y)] \\ & \times [\hat{\boldsymbol{\sigma}}^{(2)}\times(\boldsymbol{p}'+\boldsymbol{k}')]_z F_{01}^{21}(q) \\ & - \beta[\hat{\boldsymbol{\sigma}}^{(1)}\times(\boldsymbol{p}+\boldsymbol{k})]_z[\hat{\sigma}_x^{(2)}(p'_x+k'_x) \\ & - \hat{\sigma}_y^{(2)}(p'_y+k'_y)]F_{10}^{12}(q) - ([\boldsymbol{p}\times\boldsymbol{k}]\hat{\boldsymbol{\sigma}}^{(1)}) \\ & \times ([\boldsymbol{p}'\times\boldsymbol{k}']\hat{\boldsymbol{\sigma}}^{(2)})F_{22}^{00}(q)\}|\chi_s\chi_{s'}\rangle. \end{aligned} \tag{9}$$

Here we disregarded the terms with odd powers of the wavevectors and the terms with powers of the wavevectors higher than 4: odd terms do not result in a two-electron state fine structure, and the higher-order terms do not change the results qualitatively. The terms in the first and last lines of equation (9) were derived in [7], the form factor $F_{11}^{11}(q) = 3q/(4d)$. The allowance for the bulk inversion asymmetry results in new terms proportional to $\beta$ and $\beta^2$. The form factor at the $\beta^2$ terms is $F_{00}^{22}(q) = \pi^4/d^4$. Note that the terms linear in $\beta$ arise due to an interplay of bulk and structural inversion asymmetry, the corresponding form factors $F_{10}^{12}(q) = F_{01}^{21}(q) = -128\alpha q/(15d^2)$. These form factors are non-zero in asymmetric quantum wells only.

### *2.1. Allowance for the heavy–light-hole splitting*

So far, we assumed that the valence band $\Gamma_8^{\mathrm{v}}$ states are degenerate at $\boldsymbol{k} = 0$. The deformation of a cubic semiconductor along the $z$ axis lifts this degeneracy, see figure 1(b). In quantum wells the size quantization removes the degeneracy of the states with the total momentum projection $\pm 3/2$ and $\pm 1/2$ on the growth axis. A similar model can be applied to a certain extent to wurtzite semiconductors, with $z$ being the wurtzite axis [16].

In order to analyze the effect of the valence band splitting on the spin–orbit contributions to the electron–electron interaction Hamiltonian we disregard the bulk inversion

[1] These terms can be interpreted as the Rashba effect for a given electron caused by the other one. In our model they vanish because the total $z$ component of the electric field induced by some charge distribution acting on the same charge distribution is zero [26].

asymmetry (i.e. put $\beta = 0$). We denote as $E_g$ the distance between the $\Gamma_6^c$ band and a light-hole band ($z$ component of the hole angular momentum being $\pm 1/2$) and as $\tilde{E}_g$ the distance between $\Gamma_6^c$ band and a heavy-hole band ($z$-component of the angular momentum being $\pm 3/2$). Let $\Delta$ be the splitting between the light-hole band and the spin–orbit split-off band $\Gamma_7^v$, see figure 1(b). We assume that the heavy–light-hole splitting $\tilde{E}_g - E_g$ is small as compared with $\Delta$. Under this assumption function $\hat{\mu}$ in equation (5) takes the form

$$\hat{\mu}(z, \boldsymbol{k} \to \boldsymbol{p}, \hat{\boldsymbol{\sigma}}) = \varphi^2(z) + \mathrm{i}(\xi + \tilde{\xi})\hat{\sigma}_z[\boldsymbol{p} \times \boldsymbol{k}]_z \varphi^2(z) + \xi[\hat{\boldsymbol{\sigma}} \times (\boldsymbol{p} + \boldsymbol{k})]_z \varphi'(z)\varphi(z), \tag{10}$$

where $\xi$ is given by equation (4) (with the notations above) and $\tilde{\xi} = -P^2(E_g^2 - \tilde{E}_g^2)/(2E_g^2\tilde{E}_g^2)$. The splitting of the hole states results in the change of the coefficient at the term proportional to $\hat{\sigma}_z$.

### 2.2. Short-range electron–electron interaction

The method developed in [7] and extended here allows one to determine the long-range contributions to the electron–electron interaction which are caused by the Fourier components of the Coulomb potential with the transferred wavevector much smaller as compared with the inverse lattice constant. Within the framework of the effective mass method other Fourier components of the Coulomb potential $V(\boldsymbol{r})$ form a short-range electron–electron interaction:

$$\mathcal{H}^{\mathrm{short}}(\boldsymbol{r}, \boldsymbol{r}') = \gamma_{ij}\, \hat{\sigma}_i^{(1)} \hat{\sigma}_j^{(2)}\, \delta(\boldsymbol{r} - \boldsymbol{r}'), \tag{11}$$

where the summation over the repeated Cartesian subscripts $i, j = x, y, z$ is assumed. Here the spin-independent contributions are ignored and the non-zero components of the tensor $\gamma_{ij}$ are determined by the point symmetry of the considered system.

In bulk cubic semiconductors the tensor $\gamma$ reduces to the scalar and the short-range interaction equation (11) simply adds to the Coulomb exchange interaction caused by the (anti)symmetry of the wavefunctions and, hence, the short-range contribution can be disregarded. In bulk deformed semiconductors and in wurtzite systems there are two independent components of tensor $\gamma$: $\gamma_{zz}$ and $\gamma_\perp \equiv \gamma_{xx} = \gamma_{yy}$.

The effective short-range interaction Hamiltonian in low-dimensional systems—quantum wells, wires and QDs—can be obtained by the averaging of equation (11) with the size-quantization wavefunctions of interacting electrons. It is worth noting that the additional terms may arise due to the interfaces of the low-dimensional systems similar to the case of an exciton localized in type II superlattices [17]. Indeed, if a pair of electrons is localized in the vicinity of the interface, even in the case where its envelope function is isotropic, its microscopic wavefunction experiences the $C_{2v}$ point symmetry of an ideal interface. Hence, the corresponding terms should appear in the effective electron–electron interaction Hamiltonian. Evaluation of the tensor $\gamma_{ij}$ and the interface contributions requires a fully microscopic calculation.

## 3. Two-electron triplet state fine structure

Here we apply the developed formalism to calculate the fine structure of two electrons localized either in a single QD or in a lateral double QD. In what follows we consider triplet states which are described by antisymmetric combination of single-electron in-plane envelopes $\psi_1(\boldsymbol{\rho}_1)$, $\psi_2(\boldsymbol{\rho}_2)$:

$$\Psi(\boldsymbol{\rho}_1, \boldsymbol{\rho}_2) = \mathcal{N}[\psi_1(\boldsymbol{\rho}_1)\psi_2(\boldsymbol{\rho}_2) - \psi_1(\boldsymbol{\rho}_2)\psi_2(\boldsymbol{\rho}_1)], \tag{12}$$

where $\mathcal{N}$ is the normalization constant. The singlet–triplet splitting caused by the Coulomb exchange interaction is $2U_e$, where

$$U_e = \frac{2\mathcal{N}^2 e^2}{\varkappa} \int \frac{\mathrm{d}\boldsymbol{\rho}_1 \mathrm{d}\boldsymbol{\rho}_2}{|\boldsymbol{\rho}_1 - \boldsymbol{\rho}_2|} \psi_1(\boldsymbol{\rho}_1)\psi_2(\boldsymbol{\rho}_1)\psi_2(\boldsymbol{\rho}_2)\psi_1(\boldsymbol{\rho}_2). \tag{13}$$

It is assumed to exceed by far the fine structure splittings of the triplet states.

In the absence of the spin–orbit interaction the triplet state equation (12) is threefold-spin-degenerate with respect to the $z$ component of the total electron spin: $m_z = 0, \pm 1$. In the QD systems described by the $C_{2v}$ point symmetry group with the main in-plane axes $x' \parallel [1\bar{1}0]$, $y' \parallel [110]$ and the axis $z' \parallel [001]$, the effective Hamiltonian acting in the basis of the three states $|m_z\rangle$ which describes their fine structure can be represented via the operators of the total momentum 1, $\hat{S}_i$ ($i = x', y', z'$) as

$$\hat{\mathcal{H}} = \mathcal{A}\hat{S}_{x'}^2 + \mathcal{B}\hat{S}_{y'}^2 - (\mathcal{A} + \mathcal{B})\hat{S}_{z'}^2, \tag{14}$$

by means of two independent constants $\mathcal{A}$ and $\mathcal{B}$. The term proportional to $\hat{S}_z^2$ is added in order to eliminate the irrelevant total energy shift of the triplet.

There are three non-degenerate eigenstates of the Hamiltonian (14) [7]: one state with energy $\mathcal{E}_0 = \mathcal{A} + \mathcal{B}$ characterized by the total spin projection on the growth axis being 0 and 'linearly polarized' combinations:

$$|x'\rangle = \frac{1}{\sqrt{2}}(|+1\rangle + |-1\rangle), \qquad |y'\rangle = -\frac{\mathrm{i}}{\sqrt{2}}(|+1\rangle - |-1\rangle), \tag{15}$$

with energies $\mathcal{E}_{x'} = -\mathcal{B}$ and $\mathcal{E}_{y'} = -\mathcal{A}$, respectively, similar to those of heavy-hole exciton in an anisotropic quantum disc [2, 18, 19]. The values of the constants $\mathcal{A}$ and $\mathcal{B}$ depend on the wavefunction shapes and on the spin splitting parameters $\xi$, $\tilde{\xi}$ and $\beta$.

### 3.1. Single quantum dot

First we consider a single parabolic QD. As an example we take the lowest excited $SP$ triplet state where one electron occupies the ground state ($S$-shell orbital) and the other one occupies the lowest excited ($P$-shell) state:

$$\psi_1(\boldsymbol{\rho}) = \frac{1}{\sqrt{2\pi a^2}} \mathrm{e}^{-\rho^2/4a^2}, \qquad \psi_2(\boldsymbol{\rho}) = \frac{x'}{a}\psi_1(\boldsymbol{\rho}). \tag{16}$$

Here $a$ is an effective disc radius. It is assumed that the QD is slightly elongated along the $x'$ axis so that the $P_{x'}$ orbital (given by equations (16)) is lower in energy as compared

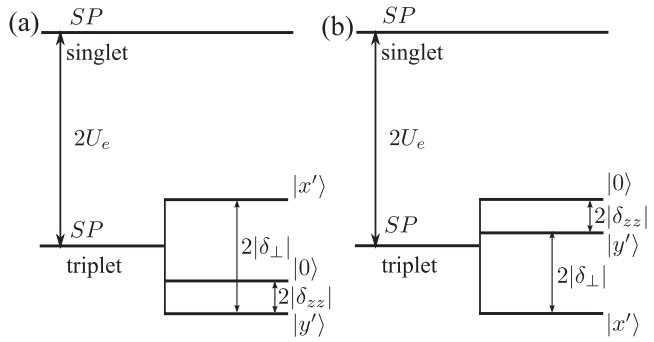


**Figure 2.** Schematic illustration of the two-electron energy level fine structure in an anisotropic quantum disc. Here $|0\rangle$, $|x'\rangle$ and $|y'\rangle$ denote spin states, equation (15). The singlet state lies above the triplet states and is not affected by the spin–orbit interaction. Panel (a): negligible structural inversion asymmetry ($\delta_\perp < 0$) and panel (b) comparable bulk and structural inversion asymmetry ($\delta_\perp > 0$). Splittings are not shown to scale.

with the $P_{y'}$ orbital with the wavefunction $(y'/a)\psi_1(\boldsymbol{\rho})$. The deformation of the wavefunctions due to the ellipticity of the QD is neglected [7]. The singlet–triplet splitting in such a QD equals $2U_e = \sqrt{\pi}e^2/(4\varkappa a)$.

The constants $\mathcal{A}$ and $\mathcal{B}$ in equation (14) can be conveniently expressed in terms of new parameters $\delta_\perp$ and $\delta_{zz}$ describing the splittings between the linearly polarized states and between the state with $m_z = 0$ and one of the linearly polarized states, namely $|y'\rangle$, respectively, as is shown in figure 2:

$$\mathcal{A} = -\tfrac{2}{3}(\delta_\perp + \delta_{zz}), \qquad \mathcal{B} = \tfrac{2}{3}(2\delta_\perp - \delta_{zz}). \tag{17}$$

The calculation of matrix elements, equation (9), with the antisymmetrized wavefunction (12) neglecting heavy–light-hole splitting shows that the direct contribution vanishes (because $M^{(2)}$ is represented as a product of operators acting on each electron state) and the exchange contribution yields

$$\begin{aligned} \delta_{zz} &= -\xi^2 \frac{\sqrt{\pi}e^2}{32\varkappa a^5}, \\ \delta_\perp &= -\xi^2 \frac{e^2}{\varkappa d}\left[\frac{3}{8a^4} + \frac{\pi^{9/2}\beta^2}{2d^3a^3} - \frac{128\alpha\beta}{15da^4}\right]. \end{aligned} \tag{18}$$

There are three contributions to $\delta_\perp$: the first one calculated in [7] is not related with the lack of an inversion center, the second one results from the bulk inversion asymmetry and the third one is a result of an interplay between the bulk and structural inversion asymmetry. Two last terms in equations (18) are zero if bulk inversion asymmetry is disregarded ($\beta = 0$), moreover, the third contribution to $\delta_\perp$ vanishes at $\alpha = 0$, i.e. if the heteropotential has an inversion center.

It follows from equations (17) and (18) that the spin degeneracy of the triplet two-electron states is fully lifted in anisotropic QDs by the combination of the exchange and spin–orbit interactions (spin–orbit exchange). In perfectly isotropic QDs the situation may be different [7].

It is worth noting that, depending on the values of $\alpha$ and $\beta$, the sign of $\delta_\perp$ can be arbitrary. The negative sign of $\delta_\perp$ corresponds to the small structural inversion asymmetry, while the positive sign of $\delta_\perp$ corresponds to the comparable bulk and structural inversion asymmetries, $\alpha\beta > 0$. In this case the last term in equations (18) becomes dominant. It results in a different order of levels: if $\delta_\perp < 0$ when the state with $m_z = 0$ lies between the states $|x'\rangle$ and $|y'\rangle$ figure 2(a), otherwise it lies above the doublet $|x'\rangle$ and $|y'\rangle$ figure 2(b). Since $\delta_{zz} < 0$ the state $|0\rangle$ always lies above the state $|y'\rangle$.

The allowance for the heavy–light-hole splitting results in the replacement of $\xi$ by $\xi + \tilde{\xi}$ in the expression for $\delta_{zz}$, equations (18). If $\tilde{E}_g < E_g$, i.e. the valence band top is determined by the heavy holes, see figure 1(b), then $|\delta_{zz}|$ increases.

### 3.2. Lateral double quantum dot

The fine structure of triplet two-electron states in lateral double QDs is qualitatively similar to the case of SP electron states in a single QD considered above.

We assume that the electron states in each dot can be described by Gaussian wavefunctions [20]:

$$\psi_1(\boldsymbol{\rho}) = \frac{1}{\sqrt{2\pi}a}e^{-\rho^2/4a^2}, \qquad \psi_2(\boldsymbol{\rho}) = \frac{1}{\sqrt{2\pi}a}e^{-(\boldsymbol{\rho}-\boldsymbol{L})^2/4a^2}, \tag{19}$$

where $\boldsymbol{L}$ is a vector connecting QD centers. The overlap between these states $\sim \exp(-L^2/4a^2)$ is supposed to be small so that the triplet state can be written in the form of equation (12). The normalization constant $\mathcal{N} = [2 - 2\exp(-L^2/4a^2)]^{-1/2} \approx 1/\sqrt{2}$. The Coulomb exchange interaction constant $U_e$ given by equation (13) is equal approximately to[2] $0.89\exp(-L^2/4a^2)e^2/(\varkappa a)$ and is assumed to exceed the fine structure splittings of the triplet state.

In what follows we disregard the bulk inversion asymmetry $\beta = 0$ and the splitting of the heavy- and light-hole bands. It is convenient to express the constants $\mathcal{A}$ and $\mathcal{B}$ in the effective Hamiltonian (14) via the parameters $\delta_\perp$ and $\delta_{zz}$ by means of equations (17). The calculation shows that[3]

$$\delta_{zz} = -0.014\frac{e^2\xi^2}{a^5\varkappa}\frac{L^2}{a^2}e^{-\frac{L^2}{4a^2}}, \qquad \delta_\perp = -\frac{3e^2\xi^2}{32da^4\varkappa}\frac{L^2}{a^2}e^{-\frac{L^2}{4a^2}}. \tag{20}$$

The qualitative level arrangement is similar to the one shown for a single QD in figure 2(a). The allowance for the bulk and structural inversion asymmetries may transform the level arrangement to the one shown in figure 2(b). In the latter case the splittings and eigenspin states are strongly sensitive to the orientation of the vector $\boldsymbol{L}$ relative to the in-plane axes.

It is instructive to analyze an interplay of the electron–electron spin–orbit exchange interaction and the spin splitting of the conduction band caused by bulk and structural inversion asymmetry. In the relevant case where the interdot distance $L$ exceeds by far the QD size $a$ the spin–orbit splitting of the conduction band can be eliminated in the lowest order by a unitary transformation which takes into account the rotation of electron spin during the electron tunneling [21, 22]. Hence, the

[2] It was obtained by fitting the results of numerical integration.

[3] The value of $\delta_{zz}$ was obtained by fitting the results of numerical integration.

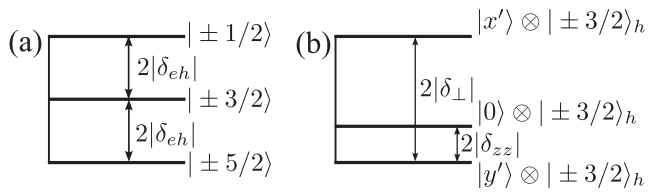


**Figure 3.** Hot trion fine structure. (a) Dominant electron–hole exchange interaction: $|\pm 1/2\rangle$, $|\pm 3/2\rangle$, and $|\pm 5/2\rangle$ denote the total spin (electron and hole) projection on the growth axis. (b) Dominant electron–electron spin–orbit exchange interaction: $|x'\rangle$, $|y'\rangle$ and $|0\rangle$ denote the two-electron spin states, equation (15), $|\pm 3/2\rangle_{\rm h}$ is the hole spin state.

exchange interaction between the electrons expressed in terms of the transformed spins has the same form as without the spin–orbit splitting, equation (14). Therefore, the level splittings are the same as without the conduction band spin splitting, but the eigenstates are different because they correspond to the rotated spins. The higher-order effects of the conduction band spin–orbit splitting may give rise to an additional contribution to $\delta_{zz}$ [22].

Finally, we compare the ratio of the spin splitting $|\delta_{zz}|$ to the exchange Coulomb interaction energy for the $SP$ state in a single QD and for the double QD:

$$\left|\frac{\delta_{zz}}{U_{\rm e}}\right| \approx \frac{\xi^2}{a^4} \times \begin{cases} 0.25, & \text{single dot,} \\ 0.016\dfrac{L^2}{a^2}, & \text{double dot.} \end{cases}$$

Therefore the relative role of the spin–orbit effects in double dots is higher: although the absolute values of the fine structure constants decrease with an increase of the dot separation $L$, the ratio of the spin splittings of the triplet and the exchange interaction constant increases.

It is worth noting that the values of the splittings depend strongly on the QD geometry and its asymmetry. In the QD ensembles with the relatively high inhomogeneous broadening the fine structure of two-electron states can manifest itself as a dephasing of the total spin of interacting electrons, similarly to the exciton spin dephasing [2].

## 4. Emission spectra

In this section we calculate the emission spectra of a single QD in two particular situations where the fine structure of triplet two-electron states is manifested: first, we consider the emission of a 'hot' (excited) trion and, second, we consider the emission of a doubly charged exciton.

### *4.1. Hot trion*

The hot trion is formed from a hole and two electrons: one in the ground and the second one in the excited state in the QD. In what follows we assume that two electrons occupy S and P orbitals and constitute the orbital state described by the antisymmetric wavefunction, equation (12). Although this state is excited, its relaxation to the ground, singlet trion state where two electrons occupy the same orbital can be strongly suppressed [5]. A fine structure of the excited trion is determined by an interplay of the electron–electron spin–orbit exchange interaction and the electron–hole exchange interaction.

The short-range part of the exchange interaction Hamiltonian between the hole and two electrons in the SP excited state is given by

$$\hat{\mathcal{H}}_{\rm eh} = \tfrac{2}{3}\delta_{\rm eh}[\hat{\sigma}_z^{(1)} + \hat{\sigma}_z^{(2)}]\hat{J}_z, \qquad (21)$$

where $\hat{J}_z$ is the heavy-hole angular momentum projection operator and $\delta_{\rm eh}$ ($\delta_{\rm eh} < 0$, as a rule) is a constant determining the splittings between the states with different $z$ components of the total spin (electron and hole), see figure 3(a). Hence, if the electron–electron spin–orbit exchange interaction is negligible, the fine structure of a triplet hot trion consists of three twofold-degenerate sublevels split by $|2\delta_{\rm eh}|$. Two of these sublevels $|\pm 1/2\rangle$ and $|\pm 3/2\rangle$ are optically active. This fine structure for a hot trion is widely accepted in the literature [3–5] and indeed holds if $|\delta_{\rm eh}| \gg |\delta_\perp|$ in equation (17).

In the opposite limiting case, $|\delta_{\rm eh}| \ll |\delta_\perp|$, the fine structure of an excited trion state is different, see figure 3(b). There are three sublevels, each of which is twofold-degenerate with respect to the hole spin projection. All these three states are optically active. At an arbitrary relation between $\delta_{\rm eh}$ and $\delta_\perp$ there are also three doubly degenerate levels which are, in general, active.

The emission spectra are calculated by using the Fermi golden rule. We assume the constant wave non-resonant excitation of the system well above the hot trion resonance energy which results in a formation of the steady-state distribution of the trion levels, $n(E_i)$, where $E_i$ are the energies of the hot trion sublevels. The optical transitions to the final states of the system, which are the single-electron states, $f = \pm 1/2$, are described by the matrix elements $M_{fi}^{\pm}$ corresponding to the emission of a photon with a given circular polarization. As a result the emission spectra in a $\sigma^+$ or $\sigma^-$ circular polarization are given by the following expression:

$$I_\pm(\omega) \propto \sum_{ij} |M_{fi}^{\pm}|^2 n(E_i)\Delta(E_i - E_f + \hbar\omega). \qquad (22)$$

Here $E_f$ are the final state energies and $\Delta(E)$ is the broadened $\delta$ function describing energy conservation in the process of photoemission. Equation (22) is valid provided the initial and final states are well defined, so that the splitting between these states exceeds their broadening; otherwise one has to use a more elaborate approach [23]. In what follows it is assumed that $n(E_i) = \text{const}$, i.e. all the initial sublevels are equally populated.

Hot trion emission spectra calculated in the case of relatively weak and relatively strong electron–electron spin–orbit exchange interactions are presented in figure 4, panels (a) and (b), respectively. Different curves which are vertically shifted for clarity correspond to different values of the magnetic field applied along the growth axis. We take into account only the Zeeman effect of the magnetic field. The electron and hole effective $g$ factors which determine the energies of the spin-split states as $\pm g_{\rm e}\mu_{\rm B}B/2$ and $\pm 3g_{\rm h}\mu_{\rm B}B/2$ (where $\mu_{\rm B}$ is the Bohr magnetron and $B$ is the magnetic field

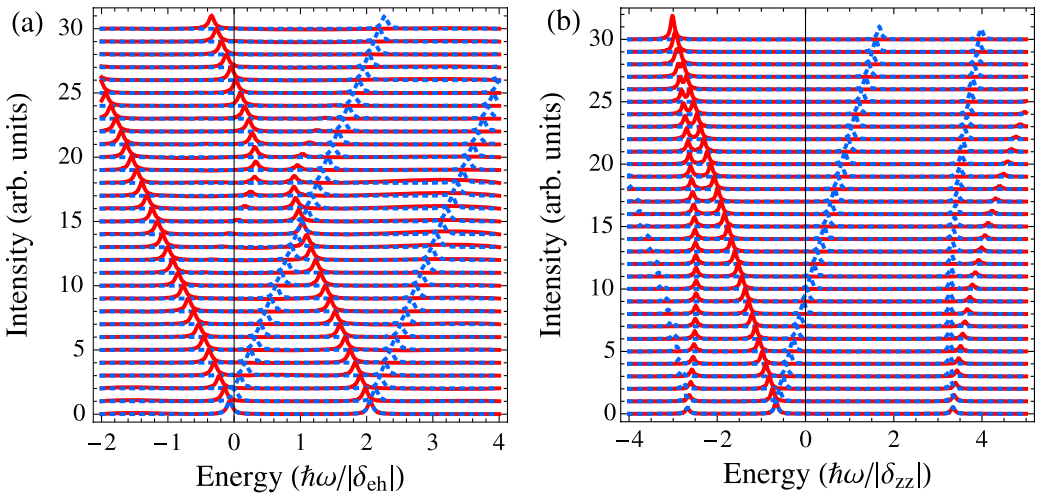


**Figure 4.** Emission spectra of a hot trion. Different lines (offset along the vertical axis for clarity) correspond to different values of an external magnetic field applied along the $z$ axis. Red/solid curve corresponds to the emission in $\sigma^+$ polarization, blue/dotted curve corresponds to the emission in $\sigma^-$ polarization. Electron and hole effective $g$ factors are $g_{\rm e} > 0$, $3g_{\rm h} = -0.42g_{\rm e}$. Panel (a): relatively small electron–electron spin–orbit exchange interaction, $\delta_{zz} = 0.1\delta_{\rm eh}$, $\delta_\perp = 3\delta_{zz}$, $\delta_{\rm eh} < 0$ and $|\delta_{\rm eh}|$ is used as a unit of energy. The energy is referred from the position of the state with the total spin $z$ component being $\pm 3/2$ calculated neglecting electron–electron spin–orbit coupling. Panel (b): relatively large electron–electron spin–orbit exchange interaction, $\delta_\perp = 3\delta_{zz}$, $\delta_{zz} < 0$, $\delta_{\rm eh} = 0.1\delta_{zz}$ and $|\delta_{zz}|$ are used as a unit of energy. The energy is referred from the center of a two-electron triplet states calculated neglecting electron–hole exchange interaction. The lines are Lorentzian broadened, $\Delta(\omega) = \pi^{-1}\Gamma/(\omega^2 + \Gamma^2)$ in equation (22), with the width $\Gamma = 0.05|\delta_{zz}|$.

$z$ component) are chosen to have different signs, $g_{\rm e} > 0$, $g_{\rm h} < 0$ which corresponds to CdSe/ZnSe/ZnMnSe QDs being studied in [24]. Other parameters are presented in the caption to figure 4.

In the case of a weak electron–electron spin–orbit exchange interaction, figure 4(a), two doublets are clearly seen which correspond to the states $|\pm 1/2\rangle$ and $|\pm 3/2\rangle$. In $B = 0$ the emission from the 'dark' states $|\pm 5/2\rangle$ cannot be seen from the figure because the bright state admixture due to electron–electron spin–orbit exchange is small. With an increase of the magnetic field an anticrossing is clearly visible, which is evidence of the electron–electron spin–orbit interaction which intermixes dark $|5/2\rangle$ and bright $|-1/2\rangle$ states when they become resonant in a certain magnetic field. The observation of such an anticrossing may allow one to measure the electron–electron spin–orbit interaction constant $\delta_\perp$.

The emission spectra are completely rearranged in the case of dominant electron–electron spin–orbit exchange interaction, $|\delta_\perp| \gg |\delta_{\rm eh}|$, figure 4(b). In this case all the states are optically active: in zero magnetic field three lines are seen, corresponding to the eigenstates shown in figure 3(b). In a magnetic field applied along the growth direction six emission lines with different intensities are visible.

### 4.2. Doubly charged exciton

Here we consider the emission spectra of a doubly charged exciton, $X^{2-}$, which is formed of three electrons and a hole. Two electrons occupy the ground $S$-shell state in a QD being in the spin singlet, and the third one occupies an excited P-orbital state. The hole occupies the ground state and radiatively recombines with one of the $S$-shell electrons, leaving the two remaining electrons in the $SP$-orbital state.

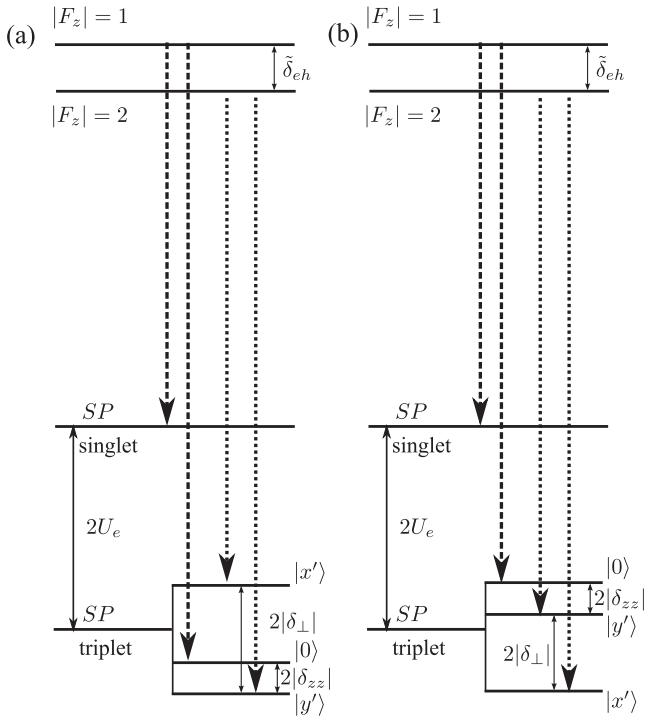


**Figure 5.** Energy levels and optical transitions in the $X^{2-}$ complex. States $|F_z| = 1$, $|F_z| = 2$ are the spin states of $X^{2-}$, while states denoted as SP singlet and triplet are the two-electron final states. Long dashed and short dashed vertical arrows denote the optical transitions from $|F_z| = 1$ and $|F_z| = 2$ states, respectively. Panel (a): negligible structural inversion asymmetry ($\delta_\perp < 0$), panel (b) comparable bulk and structural inversion asymmetry ($\delta_\perp > 0$). Splittings are not shown to scale.

The initial $X^{2-}$ state can be conveniently characterized by the $z$ component of the total spin of electrons and holes,

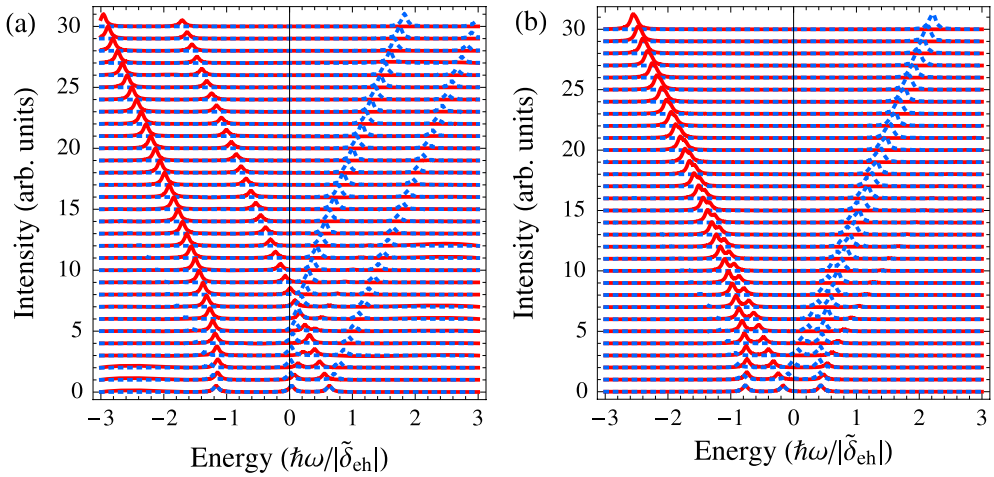


**Figure 6.** Emission spectra of the $X^{2-}$ complex. Different lines (offset along the vertical axis for clarity) correspond to different values of an external magnetic field applied along the $z$ axis. Red/solid curve corresponds to the emission in $\sigma^+$ polarization, blue/dotted curve corresponds to the emission in $\sigma^-$ polarization. Electron and hole effective $g$ factors are $g_e > 0$ and $3g_h = -0.42g_e$. The energy unit is $|\tilde{\delta}_{eh}|$. Panel (a) corresponds to the two-electron level structure shown in figures 2(a) and 5(a) where the structural inversion asymmetry is negligible: $\delta_{zz} = -0.2|\tilde{\delta}_{eh}| < 0$, $\delta_\perp = 3\delta_{zz} < 0$. Panel (b) corresponds to the two-electron level structure shown in figures 2(b), 5(b) (comparable bulk and structural inversion asymmetries): $\delta_{zz} = -0.2|\tilde{\delta}_{eh}| < 0$, $\delta_\perp = -3\delta_{zz} > 0$. The lines are Lorentzian broadened, $\Delta(\omega) = \pi^{-1}\Gamma/(\omega^2 + \Gamma^2)$ in equation (22), with the width $\Gamma = 0.05|\tilde{\delta}_{eh}|$. Transitions to singlet two-electron states are neglected.

$F_z$, which takes the following values $\pm 1$ and $\pm 2$, since two electrons form a spin singlet. The electron hole short-range exchange interaction splits the states with $|F_z| = 1$ and 2 by the value $\tilde{\delta}_{eh}$ similar to the splitting of the ground excitonic states into bright and dark doublets. In this case, however, both $|F_z| = 1$ and 2 states are optically active and the schemes of transitions for different level arrangements are depicted in figure 5.

The emission spectra shown in figure 6 are calculated for different values of the magnetic field applied along the growth axis and for two possible arrangements of two-electron triplet sublevels by using equation (22). In this case the initial, $i$, and final states, $f$, are those of the $X^{2-}$ complex and of two electrons, respectively, see figure 5. Panel (a) of figure 6 shows the case of absent structural inversion asymmetry so that the triplet sublevels order is given in figure 2(a). Panel (b) corresponds to the case of substantial bulk and structural inversion asymmetries where the triplet sublevel order is given in figure 2(b). In our calculations the transitions to the singlet two-electron states are disregarded since they are shifted in energy. We also neglect the splittings of initial states due to low symmetry of the QD.

At a zero magnetic field three lines are clearly seen which correspond to the transitions from the $|F_z| = 2$ states to the states $|x'\rangle$, $|y'\rangle$ and to the transition from the $|F_z| = 1$ states to the state $|0\rangle$ (figure 5). In weak magnetic fields the peak positions are governed by an interplay of the Zeeman splittings and the spin–orbit exchange interaction. In a relatively strong magnetic field four lines are visible. Their order and splittings are determined by the $g$ factors of carriers and by the order of two-electron final states. The emission spectra shown in figure 6 are similar to those measured in [25]. The detailed comparison of the experimental results and theory will be reported elsewhere.

## 5. Conclusions

To summarize, a theory of spin–orbit-induced terms in electron–electron interactions for the carriers confined in [001]-grown zinc blende lattice-based quantum wells and quantum dots is developed. Terms originating from the bulk inversion asymmetry and structural inversion asymmetry are derived.

The theory is applied to calculate the fine structure of two-electron states confined in a single or double QD. In anisotropic systems the spin–orbit electron–electron exchange interaction is shown to lift completely the spin degeneracy of two-electron triplet states. The analytical results are obtained for the parabolic single QDs and lateral double QDs.

We have addressed theoretically the emission spectra of two specific systems where the spin–orbit electron–electron exchange interaction may play an important role: hot trion and $X^{2-}$ complex. In the former case, the two electrons in a triplet state and a hole form an initial state of the complex. In the latter case, the two-electron state is a final one in the process of $X^{2-}$ recombination. The emission spectra of these systems in the magnetic field applied along the growth axis are calculated.

## Acknowledgments

The author thanks V D Kulakovskii and E Ya Sherman for helpful discussions. The financial support of RFBR, Programs of RAS, President Grant for young scientists and the 'Dynasty' Foundation—ICFPM is gratefully acknowledged.

## References

[1] Kusraev Y and Landwehr G (ed) 2008 *Semicond. Sci. Technol.* **23** Special Issue: Optical Orientation

[2] Ivchenko E L 2005 *Optical Spectroscopy of Semiconductor Nanostructures* (Harrow: Alpha Science)
[3] Bracker A S, Gammon D and Korenev V L 2008 *Semicond. Sci. Technol.* **23** 114004
[4] Kusrayev Y G 2008 *Semicond. Sci. Technol.* **23** 114013
[5] Cortez S, Krebs O, Laurent S, Senes M, Marie X, Voisin P, Ferreira R, Bastard G, Gerrard J-M and Amand T 2002 *Phys. Rev. Lett.* **89** 207401
[6] Ediger M, Bester G, Gerardot B D, Badolato A, Petroff P M, Karrai K, Zunger A and Warburton R J 2007 *Phys. Rev. Lett.* **98** 036808
[7] Glazov M M and Kulakovskii V D 2009 *Phys. Rev.* B **79** 195305
[8] Ivchenko E L and Pikus G E 1997 *Superlattices and Other Heterostructures* (Berlin: Springer)
[9] Knap W, Skierbiszewski C, Zduniak A, Litwin-Staszewska E, Bertho D, Kobbi F, Robert J L, Pikus G E, Pikus F G, Iordanskii S V, Mosser V, Zekentes K and Lyanda-Geller Yu B 1996 *Phys. Rev.* B **53** 3912
[10] Lawaetz P 1971 *Phys. Rev.* B **4** 3460
[11] Berestetskii V B, Pitaevskii L P and Lifshitz E M 1999 *Quantum Electrodynamics* 2nd edn, vol 4 (Oxford: Butterworth–Heinemann)
[12] Glazov M M and Ivchenko E L 2004 *JETP* **99** 1279
[13] Averkiev N S, Golub L E and Willander M 2002 *J. Phys.: Condens. Matter* **14** R271
[14] Tarasenko S A and Ivchenko E L 2005 *JETP Lett.* **81** 231
[15] Badalyan S M and Vignale G 2009 arXiv:0907.2995
[16] Bir G L and Ivchenko E L 1975 *Sov. Phys.—Semicond.* **9** 858
[17] Aleiner I L and Ivchenko E L 1992 *JETP Lett.* **55** 692
[18] Goupalov S V, Ivchenko E L and Kavokin A V 1998 *JETP* **86** 388
[19] Glazov M M, Ivchenko E L, von Baltz R and Tsitsishvili E G 2007 *Int. J. Nanosci.* **6** 265
[20] Bădescu Ş C, Lyanda-Geller Y B and Reinecke T L 2005 *Phys. Rev.* B **72** 161304
[21] Kavokin K V 2001 *Phys. Rev.* B **64** 075305
Kavokin K V 2004 *Phys. Rev.* B **69** 075302
[22] Gangadharaiah S, Sun J and Starykh O A 2008 *Phys. Rev. Lett.* **100** 156402
[23] Zora A, Simserides C and Triberis G P 2007 *J. Phys.: Condens. Matter* **19** 406201
Averkiev N S, Glazov M M and Poddubnyi A N 2009 *JETP* **108** 836
[24] Chekhovich E A, Brichkin A S, Chernenko A V, Kulakovskii V D, Sedova I V, Sorokin S V and Ivanov S V 2007 *Phys. Rev.* B **76** 165305
[25] Chekhovich E A, Brichkin A S, Chernenko A V and Kulakovskii V D 2007 *Proc. 15th Int. Symp. 'Nanostructures: Physics and Technology' (Novosibirsk)*
[26] Sherman E Ya 2009 private communication